CrossMark

Present-day status and future projection of spring Eurasian surface air temperature in CMIP5 model simulations

Shangfeng Chen[1] · Renguang Wu[1,3] · Linye Song[2] · Wen Chen[1,3]

Abstract
The present study evaluates the performance of 19 climate models that participated in the coupled model intercomparison project phase 5 (CMIP5) in reproducing climatology, the standard deviation, and the dominant mode of spring surface air temperature (SAT) variations over the mid-high latitudes of Eurasia based on historical runs. Future change of the Eurasian spring SAT under the anthropogenic global warming is also examined by comparing the historical and RCP4.5 run. All the 19 CMIP5 models capture well the observed spatial structure of climatological spring SAT, with the pattern correlation coefficients all larger than 0.94. However, most of the models tend to underestimate the SAT over north Europe and north Siberia and overestimate the SAT south of 50°N. There exists large inter-model spreads in the standard deviation of the spring SAT. Most of the models capture realistically the observed dominant mode of interannual variations of spring SAT. Analyses show that the ability of a CMIP5 model in capturing the dominant mode of Eurasian spring SAT variations is connected with the model's performance in representing the observed atmospheric circulation anomalies related to the Arctic Oscillation and the dominant mode of the atmospheric variations over Eurasia. Six best models are selected based on the ability in simulating the dominant mode of the spring SAT variations in the historical runs. These six models project an increase in the SAT climatology but a decrease in the standard deviation over most of Eurasia. These six models project a decrease in the explained variance as well as in the amplitude of the spring SAT and atmospheric anomalies related to the dominant mode.

Keywords Spring · Eurasian surface air temperature · The dominant mode · CMIP5 · Future projection

1 Introduction

Surface air temperature (SAT) is an important variable in climate variability and climate change (IPCC 2013). Anomalously high and low SAT anomalies have substantial impacts

✉ Renguang Wu
  renguang@mail.iap.ac.cn

[1] Center for Monsoon System Research, Institute of Atmospheric Physics, Chinese Academy of Sciences, Beijing 100029, China

[2] Institute of Urban Meteorology, China Meteorological Administration, Beijing, China

[3] State Key Laboratory of Numerical Modeling for Atmospheric Sciences and Geophysical Fluid Dynamics, Institute of Atmospheric Physics, Chinese Academy of Sciences, Beijing, China

on the agriculture, people's daily lives and socioeconomic development (Kunkel et al. 1999; Zeng et al. 2011; Li et al. 2014; Sun et al. 2014; Guan et al. 2015; Xia et al. 2016; Caloiero 2017). Several environmental aspects are significantly influenced by the SAT variations, such as food safety assessment, crop growth, and the agro-ecological zoning (Yao 1995; Keellings and Waylen 2012; Ye et al. 2013). For instance, the hot summer in 2003 over Europe caused substantial economic loss and casualties (Stott et al. 2004; Feudale and Shukla 2010). The extremely hot summer of 2010 over Eurasia, especially East Asia, western Russia, and Eastern Europe, has a large impact on human health and electricity source (Barriopedro et al. 2011; Matsueda 2011). Barriopedro et al. (2011) reported that the areas impacted by the extremely hot summer of 2010 exceeded the regions influenced by the previous record-breaking hot summer of 2003. In addition, the SAT change can modify the soil moisture, leading to changes in the water and energy exchange between the surface land and lower atmosphere

(Henderson-Sellers 1996). Hence, it is important to investigate the SAT variability over Eurasia and its future change.

SAT change in the Eurasian continent is impacted by several factors, such as the Arctic Oscillation (AO), the North Atlantic Oscillation (NAO), the Eurasian snow cover, Arctic sea ice and sea surface temperature (SST) change (Thompson and Wallace 1998; Gong et al. 2001; Wu and Wang 2002; Miyazaki and Yasunari 2008; Sun et al. 2008; Zveryaev and Gulev 2009; Jia and Lin 2011; Cheung et al. 2012; Chen et al. 2015, 2016; Zuo et al. 2016; Zhou and Wu 2016; Wu et al. 2016; Wu and Chen 2016; Chen and Wu 2018). Many parts of the Eurasian continent during boreal winter are covered by positive (negative) SAT anomalies in the positive (negative) phase of winter AO. Miyazaki and Yasunari (2008) suggested that the wintertime AO has a significant connection with the first empirical orthogonal function (EOF) mode of SAT variations over Asia and the surrounding oceans during boreal winter. Zuo et al. (2016) reported a close relationship between change in the sea ice over the Eurasian Arctic in September and October and the subsequent winter SAT variation in China. Chen et al. (2015) indicated that the summer northeast Asian SAT interannual variations have a close relation with the Eurasian atmospheric wave train and the East Asian Pacific atmospheric teleconnection (also called Pacific-Japan teleconnection pattern) (Nitta 1987; Huang and Sun 1992).

Climate model is an important tool to investigate the current-day climate variability and future projection. The fifth phase of the coupled model intercomparison project (CMIP5) provides substantial model outputs for the climate research (Taylor et al. 2012). Several studies have evaluated the performance of the CMIP5 models in simulating the Eurasian SAT variability (e.g., Guo et al. 2016; Xu et al. 2016). Guo et al. (2016) showed that most of the CMIP5 models capture the dominant modes of winter SAT variations over China. They further projected future change of the winter SAT over China based on the eight best models using the representative concentration pathway (RCP) 4.5 scenario. Based on the multi-model ensemble mean of the eight selected models, they reported that the winter SAT displays a nationwide warming in the future. Xu et al. (2016) investigated change in the first two EOF modes of boreal winter SAT variations over East Asia (0°–60°N and 100°–140°E) under global warming using the RCP4.5 and RCP8.5 scenarios. They showed that the explained variance of the first EOF mode (also called "northern mode"; Wang et al. 2010) will increase in most of the CMIP5 models, while the explained variance of the second EOF mode (also called "southern mode") will decrease.

Studies regarding boreal spring SAT over Eurasia are relatively less compared to those during boreal winter and summer both in the observational analyses and model simulations. It is noted that spring Eurasian SAT variations may play an important role in connecting the preceding winter atmospheric anomalies to the subsequent summer weather and climate (e.g., Ogi et al. 2003). Furthermore, spring Eurasian SAT change may influence the activity of the Asian summer monsoon through changing the ocean-continent temperature differences (e.g., Liu and Yanai 2001; D'Arrigo et al. 2006). Hence, spring Eurasian SAT variations may provide additional sources of the predictability for the following summer climate.

Chen et al. (2016) indicated that the springtime AO exerts significant influences on the first EOF mode of interannual variations of spring SAT over the mid-high latitudes of Eurasia mainly via wind-induced temperature advection. Until now, none of studies have investigated the performance of the CMIP5 models in representing the Eurasian SAT during boreal spring. Boreal spring is the time when climate models generally suffer the "predictability barrier" in association with the phase transition of the El Niño-Southern Oscillation (ENSO) (Webster and Yang 1992), which would decrease the prediction skill of the dynamical models. Therefore, it is crucial to reveal the performance of the state-of-the-art climate models from the CMIP5 in reproducing Eurasian spring SAT interannual variations. This study aims to address following issues: (1) What is the ability of CMIP5 models in capturing the present-day climatology, the standard deviation, as well as the mode of Eurasian spring SAT variations? (2) What is the key factor responsible for CMIP5 model's performance in reproducing the leading mode of Eurasian spring SAT interannual variations? (3) How will climatology, the standard deviation, and the leading mode of Eurasian spring SAT interannual variations change under global warming?

The rest of this study is organized as follows. Section 2 describes the data and methods. Section 3 investigates the ability of the CMIP5 models in reproducing the present-day climatology and standard deviation of Eurasian spring SAT. Section 4 examines the performance of the CMIP5 models in simulating the leading mode of spring Eurasian SAT interannual variations. Section 5 displays future change of the leading mode under global warming. Section 6 provides a summary of the results of the present study.

2 Data and methods

2.1 Observational data

This study employs monthly mean surface air temperature, 850 hPa winds, and 500 hPa geopotential height from the ERA-Interim (ERAINT) reanalysis (Dee 2011). The ERAINT reanalysis dataset is available from 1979 to present and has a horizontal resolution of 1.5° × 1.5°. In addition, we use the SAT from the University of Delaware (UDEL),

which is available from 1900 to 2014 on a regular 0.5° latitude–longitude grid (Matsuura and Willmott 2009). For convenience, the data obtained from ERAINT and UDEL are all called "observations".

2.2 Model data

This study uses outputs of 19 climate models from the CMIP5. Table 1 presents information of these 19 CMIP5 models, including their horizontal resolutions of the atmospheric components, institutions, and model names (More detailed information is available online at http://cmip-pcmdi.llnl.gov/cmip5/). Monthly mean surface temperature, 850 hPa winds, and 500 hPa geopotential height from CMIP5 historical and RCP4.5 simulations are analyzed. The CMIP5 historical simulations are forced by the conditions close to the observations, including greenhouse gases, solar forcing, ozone, land use, anthropogenic and natural aerosols, and volcanic influences (Taylor et al. 2012). The CMIP5 RCP4.5 simulations are used for future projection in which it is assumed that the radiative forcing will increase and reach about 4.5 W m^{-2} by the year of 2100 (Thomson et al. 2011; Taylor et al. 2012). Several CMIP5 models only have one realization of the historical and RCP4.5 experiments. For a fair comparison, the first standard run from each model is analyzed in this study. In addition, the period from 1979 to 2005 of the historical experiment is employed to compare against the observations, and the period 2073–2099 of RCP4.5 runs is used to project future change.

2.3 Methods

All the data derived from the observations, CMIP5 historical and RCP4.5 simulations are converted to a standard 0.5° latitude–longitude grid. multimodel ensemble mean (MME) is defined as the equal weighted average of individual models. A Taylor diagram is used to analyze the performance of CMIP5 models in simulating the spatial pattern of an involved variable in terms of the spatial correlation coefficient, root mean square error (RMSE), and ratio of their standard deviation (Taylor 2001). This study focuses on analyzing interannual variations, and therefore, all the data from the observations, CMIP5 historical and RCP4.5 simulations are subjected to a 9-year high pass Lanczos filter (Duchon 1979) except for the analyses of climatology and standard deviation of spring SAT. An EOF technique is used to obtain the dominant mode of spring SAT interannual variations. Spring SAT anomalies are weighted by cosine of latitude to account for the decrease of area toward the North Pole in the EOF analysis (North et al. 1982). Significant levels of correlation coefficients and anomalies obtained from regression are estimated according to the two-tailed Student's *t* test.

Table 1 Information of the 19 CMIP5 models used in this study

Model ID	Model name	Institution	HR (Lat, Lon)
a	ACCESS1-0	Commonwealth Scientific and Industrial Research Organization and Bureau of Meteorology (CSIRO-BOM), Australia	1.3° × 1.9°
b	bcc-csm1-1	Beijing Climate Center, China Meteorological Administration (BCC)	2.8° × 2.8°
c	CanESM2	Canadian Centre for Climate Modeling and Analysis, Canada	2.8° × 2.8°
d	CCSM4	Community Climate System Model, version 4	0.9° × 1.3°
e	CNRM-CM5	Centre National de Recherches Meteorologiques/Centre Europeen de Recherches et de Formation Avancee en Calcul Scientifique (CNRM-CERFACS), France	1.4° × 1.4°
f	FGOALS-s2	LASG, IAP, China	1.3° × 1.9°
g	GFDL-CM3	NOAA, GFDL	2.0° × 2.5°
h	GFDL-ESM2G	NOAA, GFDL	2.0° × 2.5°
i	GFDL-ESM2M	NOAA, GFDL	2.0° × 2.5°
j	HadGEM2-CC	Met Office Hadley Centre, United Kingdom	1.3° × 1.9°
k	HadGEM2-ES	Met Office Hadley Centre, United Kingdom	1.3° × 1.9°
l	IPSL-CM5A-LR	Institut Pierre-Simon Laplace (IPSL)	1.9° × 3.8°
m	IPSL-CM5B-LR	Institut Pierre-Simon Laplace (IPSL)	1.9° × 3.8°
n	MIROC-ESM	JAMSTEC, AORI, and NIES, Japan	2.8° × 2.8°
o	MIROC-ESM-CHEM	JAMSTEC, AORI, and NIES, Japan	2.8° × 2.8°
p	MIROC5	AORI, NIES, JAMSTEC, Japan	1.4° × 1.4°
q	MPI-ESM-LR	Max Planck Institute for Meteorology (MPI-M), Germany	1.9° × 1.9°
r	MRI-CGCM3	Meteorological Research Institute (MRI), Japan	1.1° × 1.1°
s	NorESM1-M	Norwegian Climate Centre, Norway	1.9° × 2.5°

3 Climatology and standard deviation of the spring SAT in historical runs

In this section, we first evaluate the performance of the CMIP5 models in representing climatology and the standard deviation of spring Eurasian SAT during the period of 1979–2005 based on historical simulations. Figure 1 displays climatology and the standard deviation of original spring (March–May-averaged, MAM) SAT over the mid-high latitudes of Eurasia in observations. Results obtained from the ERAINT (Fig. 1a, c) are in high agreement with those derived from the UDEL (Fig. 1b, d). Figures 2 and 3 display climatology and the standard deviation of spring SAT over Eurasia in the 19 CMIP5 models, respectively.

Relatively low climatological spring SAT appears over the north Siberia and the Russian Far East, and SAT increases southwestward with the largest values located east of the Caspian Sea (Fig. 1a, b). Large standard deviation of spring SAT extends from the Russian Far East and south of Kala Sea southward to around 50°N (Fig. 1c, d). Relatively small standard deviation appears over Europe, north China, and southeast part of Russian (Fig. 1c, d).

The MME reproduces well the spatial distribution and amplitude of climatological spring SAT. The values are small over north Siberia and Russian Far East and increase

southwestward (Fig. 2a). In particular, the MME generally captures the location of the largest value east of the Caspian Sea and the southwestward extension of a cool center around the Baikal Lake (Fig. 2a). However, the 0 °C isotherm is displaced southwestward in MME compared to that in the observations (Figs. 1a, b, 2a). A difference map (Figure S1 in the Supplementary Materials) between the observed and simulated climatological spring SAT indicates that the MME tends to underestimate climatological spring SAT in the region extending southeastward from north Europe to southeast of the Baikal Lake by about 2–3 °C, and overestimate it over a region around the Caspian Sea by about 2 °C.

Most of individual models reproduce the spatial distribution of climatological spring SAT. Difference maps (Figure S1 in the Supplementary Materials) show that climatological spring SAT over most part of Siberia is underestimated by about 4 °C in CanESM2, CNRM-CM5, GFDL-CM3, GFDL-ESM2G, HadGEM2-CC, IPSL-CM5A-LR, IPSL-CM5B-LR, MIROC-ESM, MIROC-ESM-CHEM, MIROC5, and MRI-CGCM3. The CanESM2, CCSM4, CNRM-CM5, HadGEM2-CC, HadGEM2-ES, MIROC-ESM-CHEM, and NorESM1-M underestimate climatological spring SAT over most of the Russian Far East. By contrast, climatological SAT over the Russian Far East is overestimated in bcc-csm1-1, GFDL-ESM-2M,
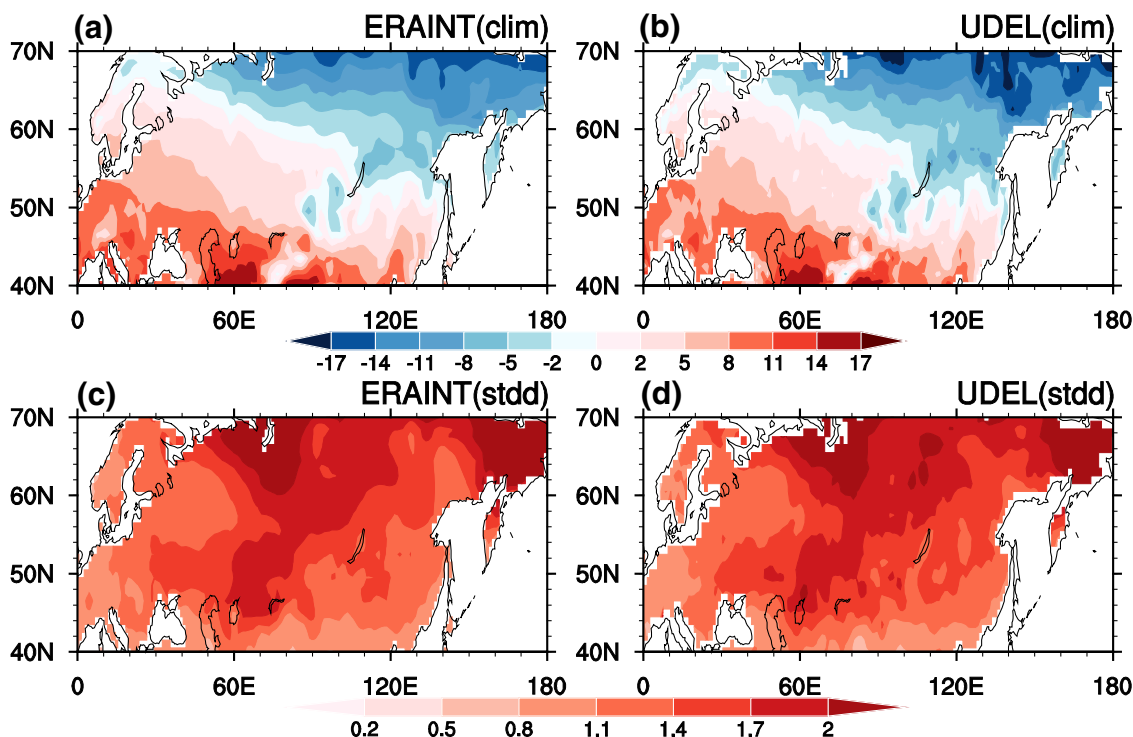

Fig. 1 **a** Climatology (°C) and **c** standard deviation (°C) of spring SAT during 1979–2005 obtained from ERAINT. **b** and **d** are the same as **a** and **c** except for SAT derived from UDEL
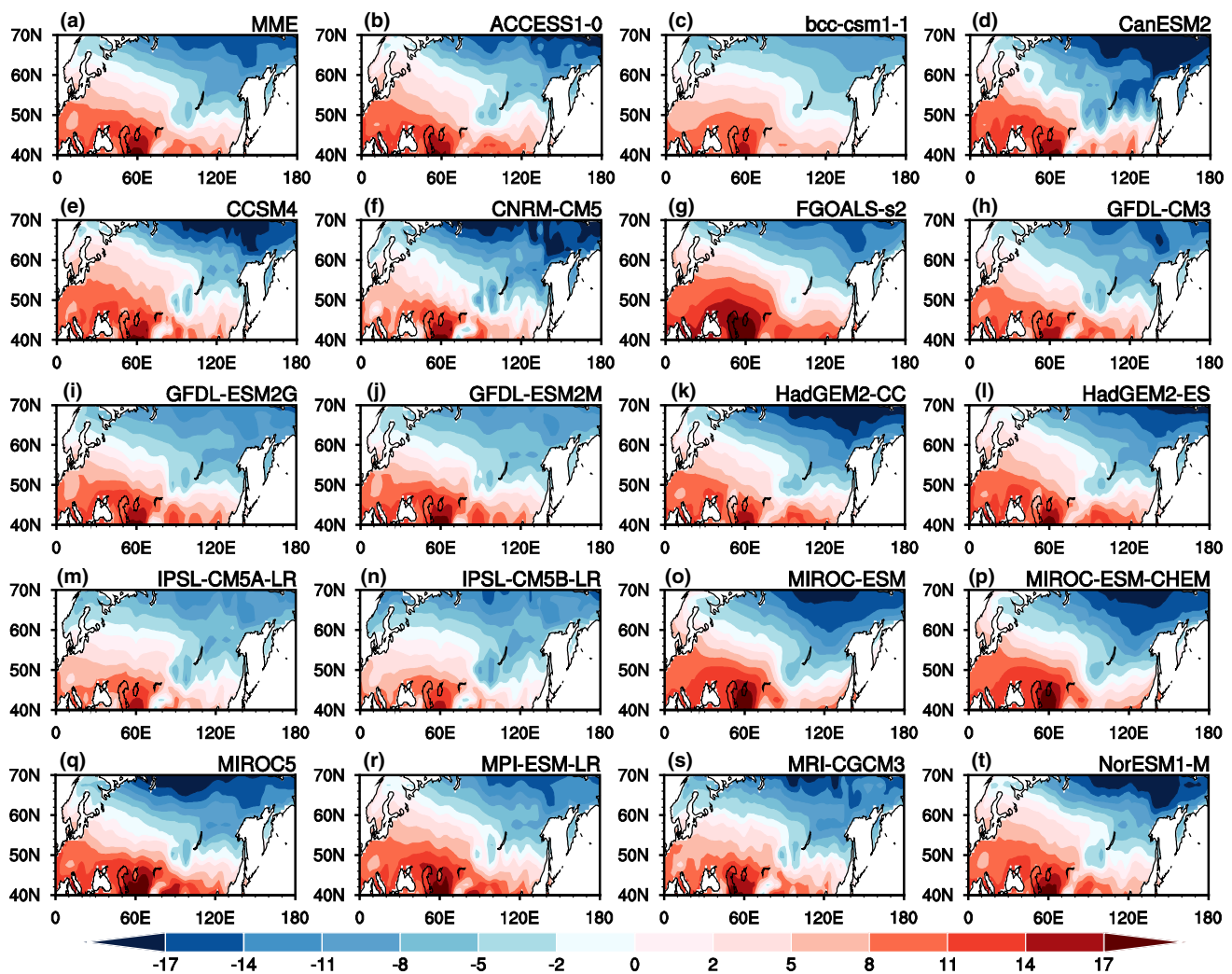
Fig. 2 Climatology (°C) of spring SAT during 1979–2005 in CMIP5 historical simulations. **a** MME of 19 CMIP5 models, **b–t** individual models

IPSL-CM5A-LR, and IPSL-CM5B-LR. In addition, most of the CMIP5 models tend to overestimate climatological spring SAT around the Caspian Sea (Figure S1).

For the standard deviation of spring SAT variations over the mid-high latitudes of Eurasia, the MME reproduces reasonably the observed spatial feature, with relatively large values over the Russian Far East and the East Siberia (Fig. 3a). A difference map (Figure S2) indicates that the variance of the spring SAT in MME is larger than observations in the region extending southeastward from north Europe to east European plain. By contrast, the variance of spring SAT over most parts of the Russian Far East is underestimated in the MME. Most of the 19 individual models cannot realistically capture the spatial distribution of the spring SAT variance. Difference maps (Figure S2) indicate that most of the models underestimate the variance of spring SAT over the Russian Far East and overestimate it over the north Europe and north part of East Siberia.

To estimate quantitatively the performance of the CMIP5 models in reproducing the observed climatological spring SAT, a Taylor diagram is presented in Fig. 4a. The pattern correlation coefficients are larger than 0.94 in individual models (Fig. 4a). This indicates that all of the 19 CMIP5 models reproduce well the spatial feature of climatological spring SAT. The ACCESS1-0 is the best model in terms of the pattern correlation coefficient (Fig. 4a). The normalized standard deviation ranges from 0.9 to 1.5. Most of the CMIP5 models overestimate the spatial standard deviations except for bcc-csm1-1, IPSL-CM5A-LR, and IPSL-CM5B-LR (Fig. 4a). The MME is better than most of the individual models in representing climatological spring SAT, with a pattern correlation coefficient of 0.98 and a normalized standard deviation of 1.2 (Fig. 4a).

A Taylor diagram is constructed to estimate objectively the ability of the CMIP5 models in representing the standard deviation of the spring SAT over the mid-high latitudes
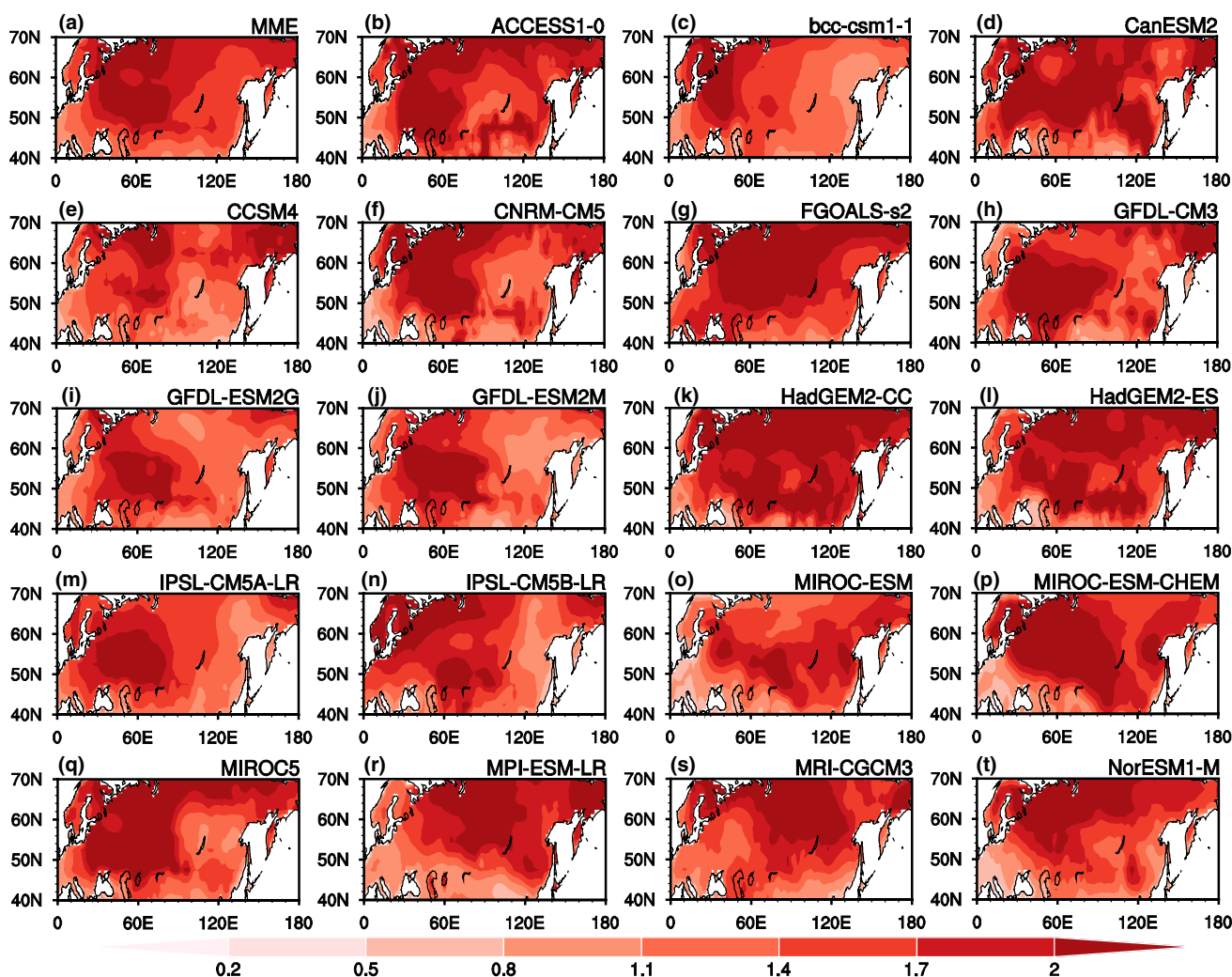
Fig. 3 Standard deviation (°C) of spring SAT during 1979–2005 in CMIP5 historical simulations. **a** MME of 19 CMIP5 models, **b–t** individual models

of Eurasia (Fig. 4b). Compared to climatology (Fig. 4a), inter-model spreads of the pattern correlation coefficients and normalized standard deviation of the standard deviation among the 19 CMIP5 models are much larger (Fig. 4b). The pattern correlations of spring SAT standard deviation range from 0.22 to 0.76, which are lower than those of the climatology (Fig. 4a, b). The pattern correlation coefficients are less than 0.25 in ACCESS1-0, GFDL-ESM2G, and GFDL-ESM2M (Fig. 4b). The CCSM4, HadGEM2-ES, and MPI-ESM-LR are the three best models in capturing the standard deviation of the spring SAT over Eurasia in terms of the pattern correlation coefficients (all larger than 0.7) (Fig. 4b). Furthermore, the normalized standard deviation ranges from 0.8 to 1.3. Similar to the climatology, the MME tends to have a better skill than most of the individual models in simulating the variance of the spring SAT over Eurasia with a pattern correlation

coefficient of 0.7 and a normalized standard deviation of 0.75.

4 Leading mode of spring SAT interannual variation over Eurasia

In this section, we analyze the performance of the 19 CMIP5 models in simulating the leading mode of the spring SAT interannual variations over the mid-high latitudes of Eurasia via an EOF analysis. The leading mode of spring SAT variations is first examined in the observations. Figure 5 displays the first EOF mode of Eurasian spring SAT variations obtained from the ERAINT and UDEL.

The distribution of the first EOF modes obtained from the ERAINT and UDEL is in high agreement with each other. The correlation coefficient between the PC time series
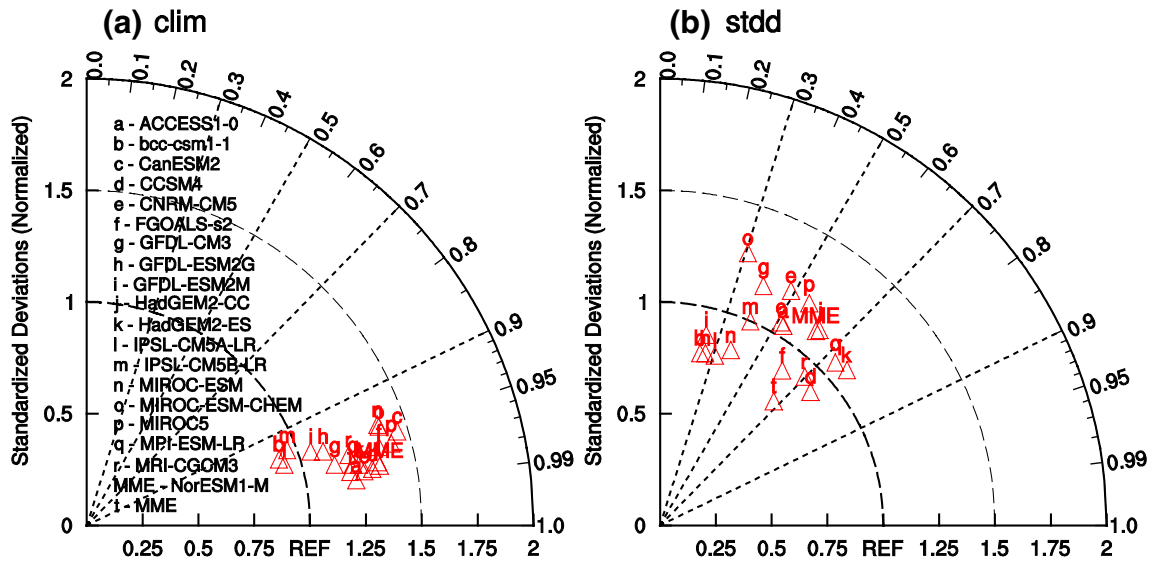
Fig. 4 Taylor diagram of **a** climatology and **b** standard deviation of spring SAT over the region of 40°–70°N and 0°–180°E. English letters "a"–"s" correspond to individual CMIP5 models ID as listed in Table 1. The pattern correlation between the CMIP5 models and ERAINT is represented by the azimuthal position. The radial distance denotes the ratio of the standard deviation obtained from CMIP5 models to the standard deviation derived from ERAINT
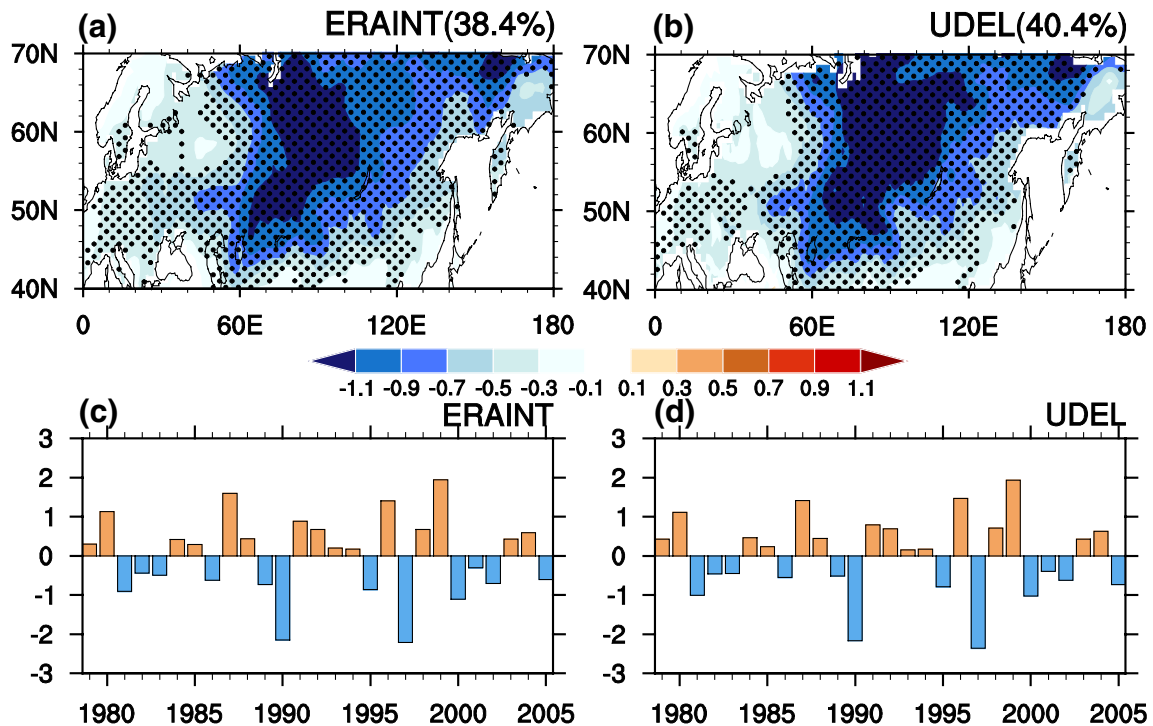

Fig. 5 Anomalies of spring SAT obtained by regressed upon the normalized PC time series of the first EOF mode of spring SAT interannual variations over 40°–70°N and 0°–180°E in **a** ERAINT and **b** UDEL during 1979–2005. **c** and **d** are the corresponding normalized PC time series of the first EOF modes of spring SAT obtained from ERAINT and UDEL, respectively. Anomalies that are significantly different from zero at the 95% confidence level are stippled in **a, b**

derived from ERAINT and UDEL is as high as 0.99 (Fig. 5c, d). Same-sign SAT anomalies are observed over most parts of the Eurasian mid-high latitudes, with a center of action located to the northwest of the Baikal Lake and relatively weak anomalies over north Europe (Fig. 5a, b). These results are generally consistent with Chen et al. (2016). Chen et al. (2016) identified the dominant mode of the spring Eurasian SAT interannual variation based on the National Centers for Environmental Prediction–U.S. Department of Energy (NCEP–DOE) during 1979–2010 (Kanamitsu et al. 2002). The corresponding PC time series shows obvious interannual variations both in the ERAINT and UDEL (Fig. 5c, d).

Chen et al. (2016) have demonstrated that formation of the leading mode of the Eurasian spring SAT variations is closely related to change in the atmospheric circulation over Eurasia. Specifically, the PC time series of the first

EOF mode of Eurasian spring SAT has a close connection with the PC time series of the first EOF mode of 500 hPa geopotential height anomalies over Eurasian region as well as with the spring AO index. Figure 6 displays anomalies of spring 850 hPa winds and 500 hPa geopotential height obtained by regression upon the normalized PC time series of the first EOF mode of spring Eurasian SAT variations. Pronounced cyclonic circulation anomalies are observed over south Europe and around the Baikal Lake, and an anomalous anticyclone extends northeastward from north Europe to Barents–Kara Sea (Fig. 6a). Correspondingly, marked anomalous northeasterly winds are present over large parts of the Eurasian mid-high latitudes (Fig. 6a). As demonstrated by Chen et al. (2016), these marked anomalous northeasterly winds carry colder air from the higher latitudes and lead to pronounced negative SAT anomalies over

Fig. 6 Anomalies of spring **a** 850 hPa winds (m s^{-1}) and 500 hPa geopotential height (m) regressed upon the normalized PC time series of the first EOF mode of spring SAT over 40°–70°N and 0°–180°E derived from the ERAINT during 1979–2005. Winds anomalies in either component that are significantly different from zero at the 95% confidence level are shaded. Geopotential height anomalies that are significantly different from zero at the 95% confidence level are stippled
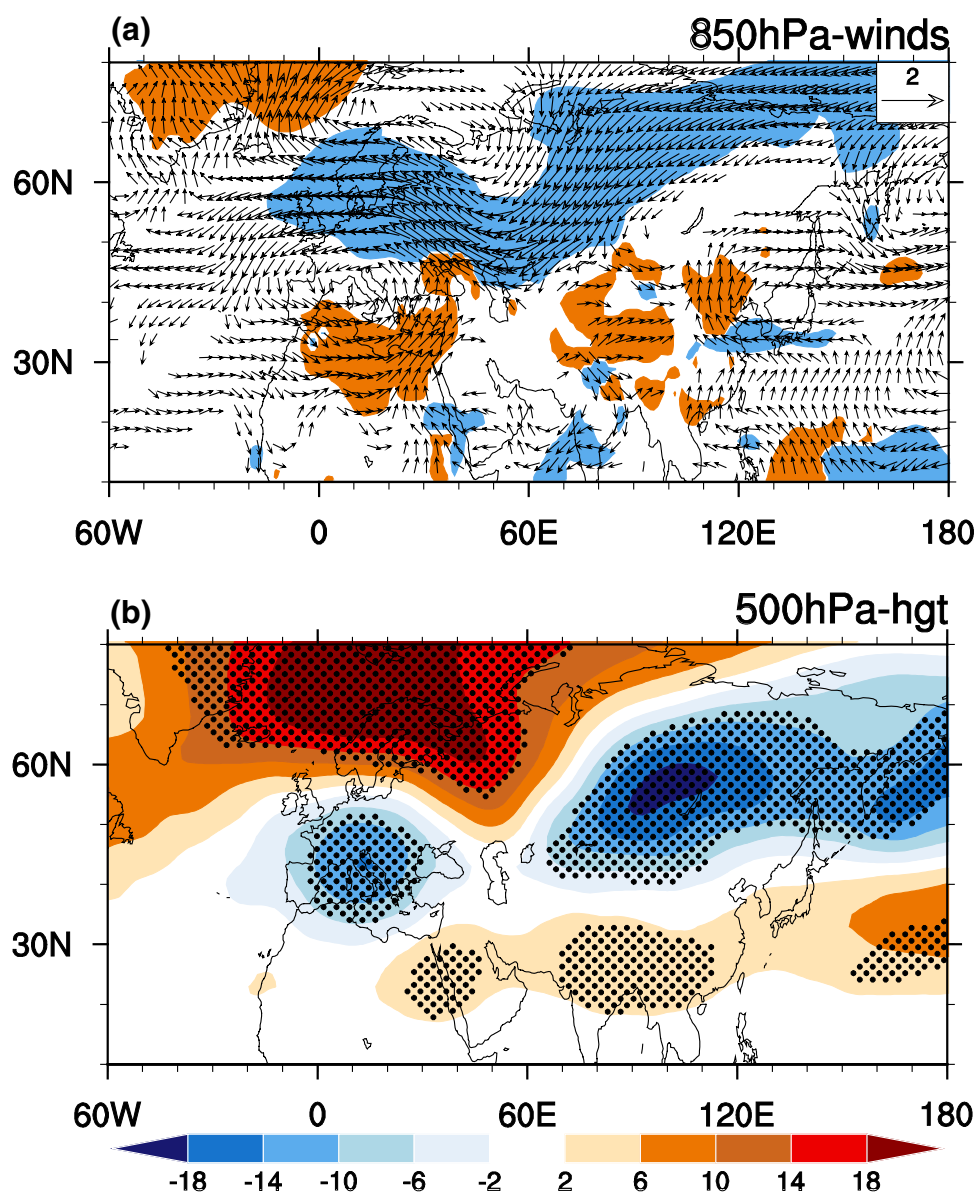
most parts of the Eurasia. The cyclonic circulation anomalies over the south Europe and around the Baikal Lake are associated with increase in the total cloud cover, which may partly contribute to negative SAT anomalies there via reducing the shortwave radiation reaching the surface (Chen et al. 2016). By contrast, the relatively weak SAT anomalies over north Europe (Fig. 5a, b) may be related to the anomalous anticyclone there. This anomalous anticyclone leads to less cloud cover and results in enhancement of net downward surface shortwave radiation (Chen et al. 2016). At 500 hPa, pronounced positive geopotential height anomalies extend northward from north Europe to the Arctic Ocean, and eastward from the northeast Africa to the western North Pacific. In addition, two centers of marked negative geopotential height anomalies are present over south Europe and around the Baikal Lake (Fig. 6b), corresponding to cyclonic circulation anomalies there (Fig. 6a). Comparison of Fig. 6a with Fig. 6b shows that the atmospheric anomalies related to the EOF1 of spring Eurasian SAT variations display a vertically barotropic structure, consistent with Chen et al. (2016).

How is the ability of the CMIP5 models in representing the leading mode of spring SAT over the mid-high latitudes of Eurasia? Fig. 7 displays the explained variance of the first EOF mode of interannual variations of Eurasian spring SAT in the 19 CMIP5 models and their MME. Figure 8 shows the associated spatial distributions of the first EOF mode. Figure 9 shows locations of the center corresponding to the maximum negative SAT anomalies over Eurasia in Fig. 8. The explained variance of the first EOF mode in MME is close to that in the observations. The bcc-csm1-1, GFDL-CM3, HadGEM2-CC, IPSL-CM5A-LR, MIROC-ESM-CHEM, MPI-ESM-LR, MRICGCM3, and NorESM1-M reproduce larger explained variances (Fig. 7). By contrast, other 11 CMIP5 models underestimate the explained variances (Fig. 7).

The MME is generally able to reproduce the same-sign SAT anomalies over most parts of Eurasia, with a center of negative SAT anomalies over the east Siberia (Fig. 8a). However, the MME underestimates the magnitude of the negative SAT anomalies over the Russian Far East, and overestimates that over the north Europe (Fig. 8a), which may be related to the biases in simulating the standard deviation of the spring SAT variations (Fig. 3a, Figure S2). In addition, the center of the negative SAT anomalies over Eurasia shifts southwestward in the MME compared to that in the observations (Fig. 9). Majority of the 19 CMIP5 models capture well the observed same-sign SAT anomalies over Eurasia. The ACCESS1-0, bcc-csm1-1, GFDL-ESM2G, IPSL-CM5B-LR, and MIROC5 have some difficulties in reproducing the spatial structure of the first EOF mode (Fig. 8b, c, i, n, q). Specifically, ACCESS1-0, bcc-csm1-1 and IPSL-CM5B-LR reproduce a dipole SAT anomaly pattern over Eurasia (Fig. 8b, c, n). The spring SAT anomaly related to the first EOF mode in MIROC5 shows a tripole pattern, with positive SAT anomalies over west and east Eurasia and negative anomalies over central Europe (Fig. 8q). Centers of the negative SAT anomalies over Eurasia in the observations and MME are around 91.5°W, 57.5°N and 64.5°W, 54.5°N, respectively (Fig. 9). Hence, the longitudinal bias (about 27°) is larger than the latitudinal bias (about 3°) in the MME (Fig. 9). For the individual models, the CanESM2 is the best model in capturing the maximum SAT anomaly center over Eurasia (Fig. 9). The HadGEM2-CC, HadGEM2-ES, MPI-ESM-LR, and MRI-CGCM3 reproduce a more eastward displacement of the negative SAT anomaly center (Fig. 9). Other 15 models simulate a westward shift of the negative SAT anomaly center (Fig. 9). In comparison, the longitudinal spread (with a range of about 75°) is larger than the latitudinal spread (with a range of about 20°) among the 19 CMIP5 models (Fig. 9).

Fig. 7 Variance explained by the first EOF mode of spring SAT interannual variation over 40°–70°N and 0°–180°E in observations and CMIP5 historical simulations during 1979–2005. Observations denote the average between ERAINT and UDEL. Vertical error bar indicates standard deviation of inter-model variability
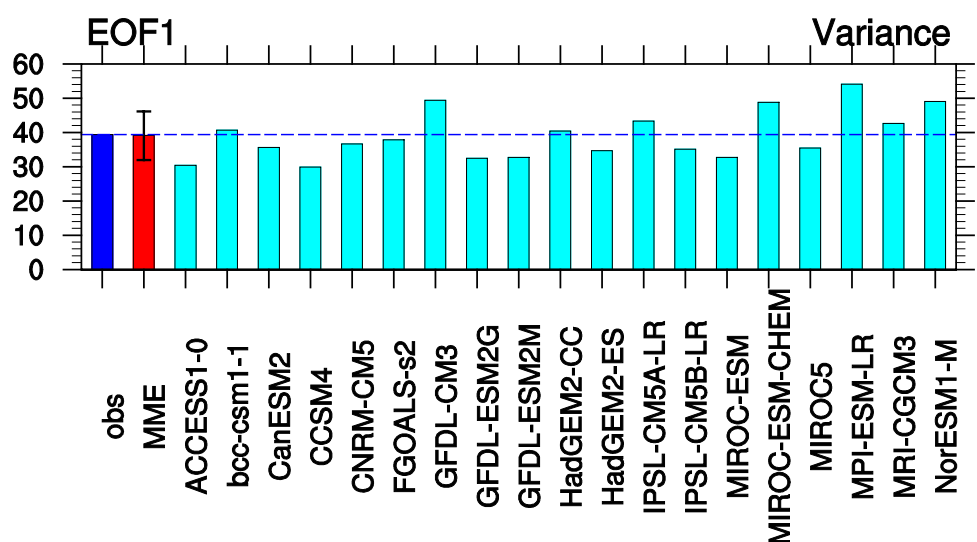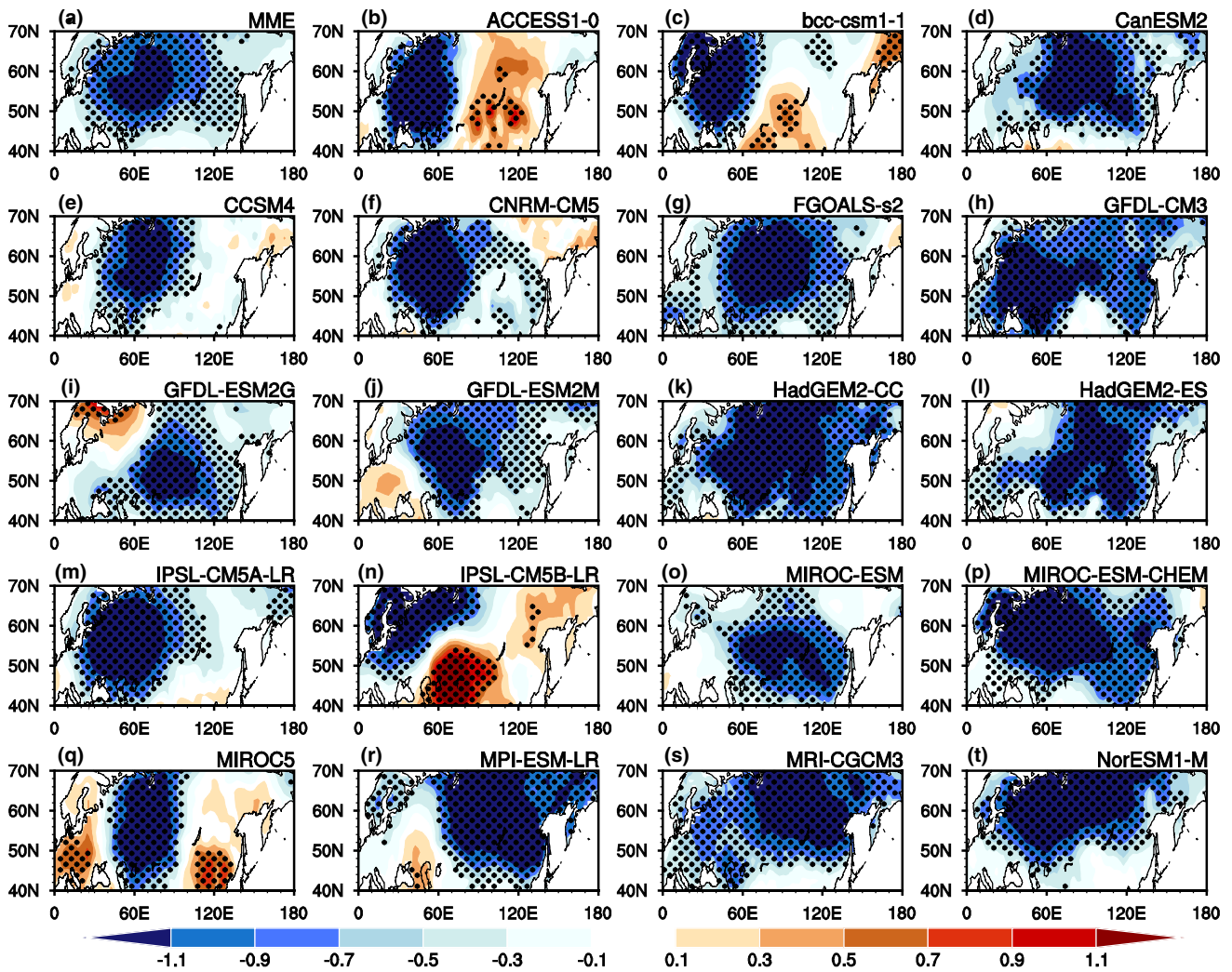
Fig. 8 Anomalies of spring SAT obtained by regressed upon the normalized PC time series of the first EOF mode of spring SAT interannual variation over 40°–70°N and 0°–180°E in CMIP5 historical simulations during 1979–2005. **a** MME of 19 CMIP5 models, **b**–**t** CMIP5 individual models. Anomalies that are significantly different from zero at the 95% confidence level are stippled in **a**–**t**
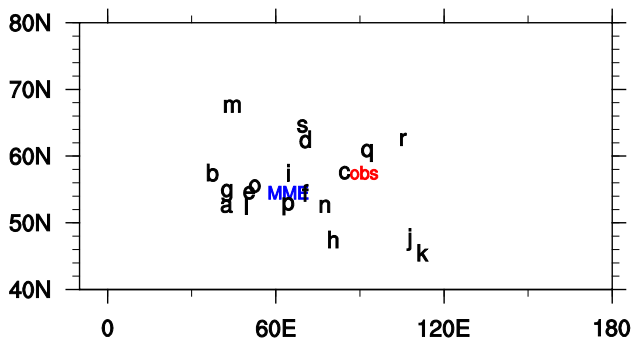

Fig. 9 Locations (latitude and longitude) of the center corresponding to the maximum negative SAT anomalies over the Eurasia as shown in Fig. 8. English letters "a"–"s" correspond to individual CMIP5 models as listed in Table 1. *MME* denotes MME of 19 CMIP5 models. *obs* represents observational result

To estimate quantitatively the performance of the 19 CMIP5 models in representing the first EOF mode of spring Eurasian SAT variations, a scatter diagram between the normalized RMSE and pattern correlation coefficient is shown in Fig. 10. The normalized RMSE ranges from 0.25 to 0.96. The pattern correlation ranges from −0.28 to 0.77. The HadGEM2-CC is the best model in simulating the first EOF mode of spring SAT variations in terms of the pattern correlation. There is a pronounced linear relationship between the normalized RMSE and the pattern correlation, with the correlation coefficient being −0.91 (Fig. 10), significant at the 95% confidence level according to the two-tailed Student's *t* test.

In the following, we analyze the possible reasons responsible for the varying ability of the 19 CMIP5 models in reproducing the first EOF mode of Eurasian spring SAT
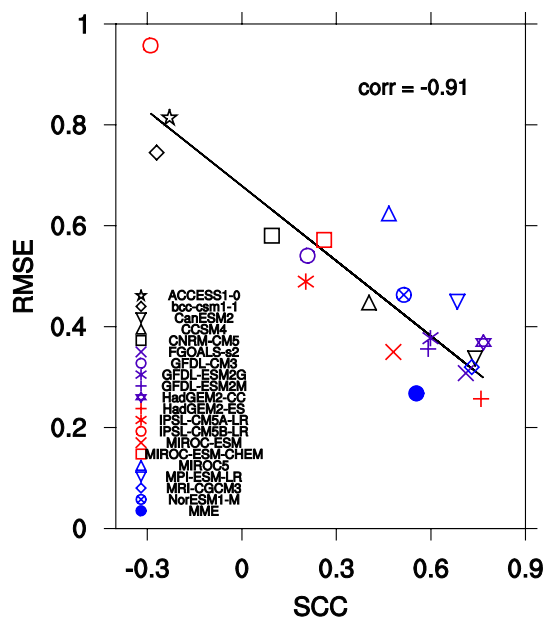
Fig. 10 Performances of 19 CMIP5 models and their MME in representing the spatial distribution of the spring SAT anomalies over Eurasia (40°–70°N and 0°–180°E) according to a scatter diagram between normalized RMSE and pattern correlation coefficient

variations. High and low correlation model groups are selected in terms of the pattern correlation. According to the pattern correlation in Fig. 10, CanESM2, FGOALS-s2, HadGEM2-CC, HadGEM2-ES, MRI-CGCM3, and MPI-ESM-LR are selected as the high correlation (HC) models (with pattern correlations larger than 0.68), and ACCESS1-0, bcc-csm1-1, CNRM-CM5, IPSL-CM5A-LR, IPSL-CM5B-LR, GFDL-CM3 and MIROC-ESM-CHEM are defined as the low correlation (LC) models (with pattern correlations less than 0.26). Figure 11 compares MME anomalies of spring SAT, 850 hPa winds, and 500 hPa geopotential height between HC and LC groups.

Substantial differences are found over Eurasia between the HC and LC groups. In the MME of HC group, significant negative SAT anomalies are present over most parts of the Eurasian mid-high latitudes except for the north Europe (Fig. 11a), consistent well with the observations (Fig. 5a, b). Pronounced positive SAT anomalies are seen over the Greenland (Fig. 11a). Significant anticyclonic circulation anomalies are seen over north Eurasia and around Japan, and pronounced cyclonic circulation anomalies are present over south Europe and around the Baikal Lake (Fig. 11c). As a result, the mid-high latitudes of Eurasia are covered by notable northeasterly wind anomalies (Fig. 11c), which explain the formation of significant negative SAT anomalies (Fig. 11a). Geopotential height anomalies at 500 hPa are featured by two centers of significant anomalies over south Europe and around the Baikal Lake, respectively, and

pronounced positive anomalies over south Japan and the Arctic region (Fig. 11e). In general, spatial patterns of the spring SAT and atmospheric circulation anomalies in the HC group bear a close resemblance to those in the observations (Figs. 5, 6, 11a, c, e).

In the MME of LC group, center of significant negative SAT anomalies shifts northwestward to East Europe (Fig. 10b), which is markedly different from that in the observations and HC group MME (Figs. 5, 11a). The corresponding atmospheric circulation anomalies in the LC group MME show an anomalous anticyclone over the Norwegian Sea and a pronounced anomalous cyclone over East Europe, with significant northeasterly wind anomalies over north Europe and the Barents–Kara Sea (Fig. 11d). The 500 hPa geopotential height anomalies show a significant dipole anomaly pattern, with significant negative anomalies over East Siberia and positive anomalies around the Norwegian Sea (Fig. 11f). Above differences between the HC and LC groups imply that the ability of the CMIP5 models in reproducing the dominant mode of Eurasian spring SAT may be closely related to the performance of the models in capturing the observed atmospheric circulation pattern.

The above assertion is verified by the relationship between the pattern correlations of SAT and height anomalies. Figure 12a displays a scatter diagram of the pattern correlation of SAT anomalies against the pattern correlation of 500 hPa geopotential height anomalies over Eurasian region (40°–70°N and 0°–180°E). Similarly, Fig. 12b shows a scatter diagram of the pattern correlation of SAT anomalies against the pattern correlation of 850 hPa meridional wind anomalies over Eurasia. Results in Fig. 12 suggest that the CMIP5 models that have larger pattern correlations of 500 hPa geopotential height and 850 hPa meridional wind anomalies tend to have larger pattern correlation of SAT anomalies over the mid-high latitudes of Eurasia. The correlation coefficients between the two variables presented in Fig. 12a, b are as high as 0.95 and 0.94, respectively, which are significant at the 99% confidence level according to the Student's *t* test. These evidences confirm the assertion that CMIP5 model's performance in representing the SAT anomalies related to the first EOF mode is closely associated with the model's ability in capturing the atmospheric circulation anomaly pattern over the Eurasia.

Above result is consistent with the finding of Chen et al. (2016). Chen et al. (2016) reported that SAT variations over Eurasia are mainly controlled by the atmospheric circulation changes. In particular, they reported that the spring Eurasian SAT anomalies related to the EOF1 mode have a close connection with the spring AO-related atmospheric circulation changes. In addition, from Fig. 11, the MME anomalies of the atmospheric circulation in the high correlation models bear some resemblance to those related to the negative phase of the spring AO (Chen et al. 2014,
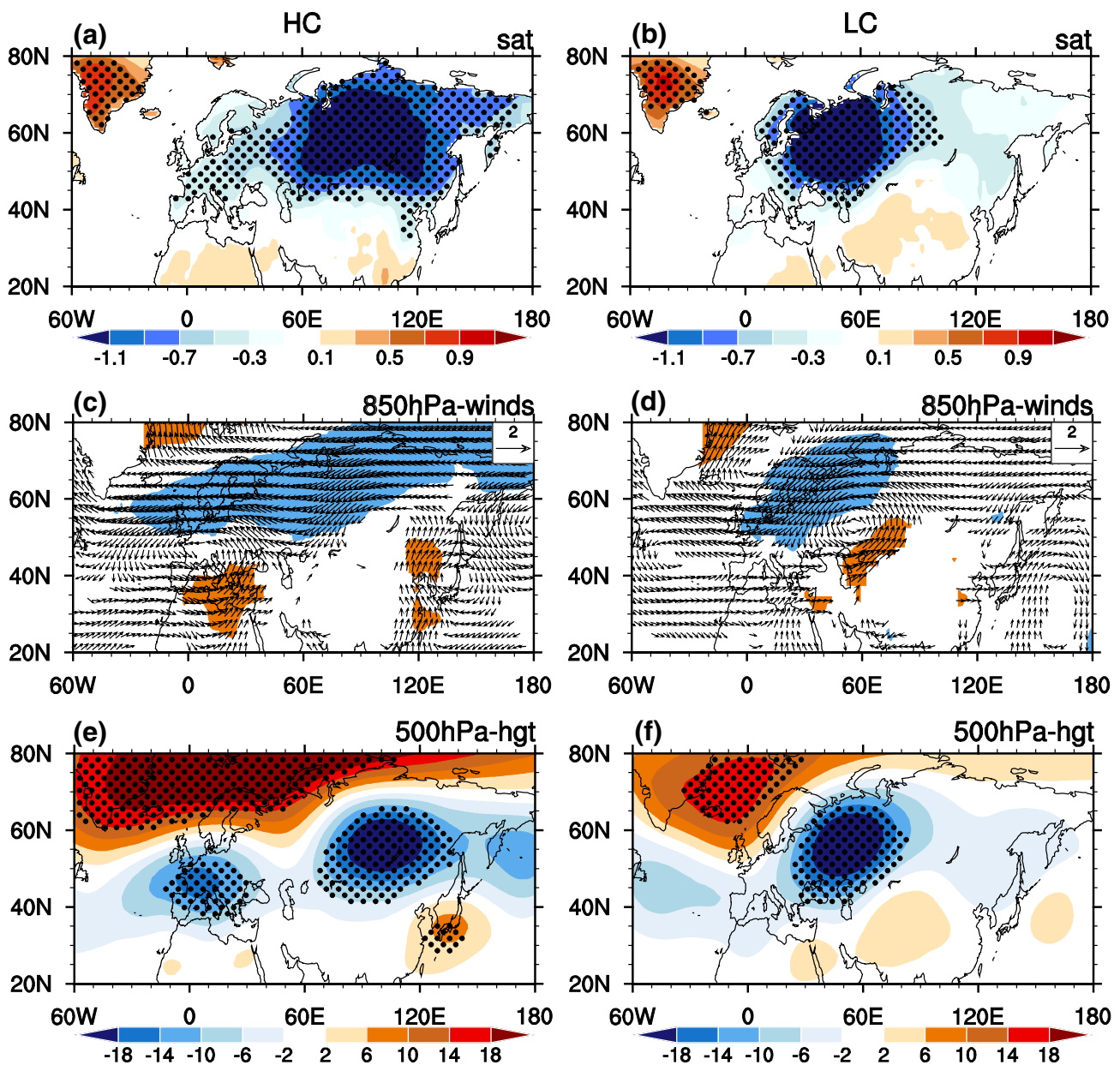
Fig. 11 MME anomalies of spring **a, b** SAT (°C), **c, d** 850 hPa winds (m s⁻¹), and **e, f** 500 hPa geopotential height (m) obtained by regression upon the normalized PC time series of the first EOF mode of spring Eurasian SAT in the (left column) HC and (right column) LC groups, respectively. Anomalies that are significantly different from zero at the 95% confidence level are stippled in **a, b** and **e, f**. Winds anomalies in **c, d** of either component that are significantly different from zero at the 95% confidence level are shaded

2016), with significant positive geopotential height anomalies over the high latitudes and negative anomalies over the mid-latitudes of the Northern Hemisphere (Fig. 11e). By contrast, the MME anomalies of the 500 hPa geopotential height in the low correlation models are different from those related to the spring AO. This notable difference in the atmospheric circulation anomalies implies that the ability of the CMIP5 model in simulating the first EOF mode of the spring Eurasian SAT anomalies may be partly related to the model's performance in capturing

connection of the EOF1 mode with the spring AO. To confirm this assertion, we calculate the correlation coefficients between the spring AO index and the PC1 time series of the spring Eurasian SAT in the high and low models (Fig. 13). Similar to observations (Chen et al. 2014, 2017), the spring AO index in the CMIP5 model is defined as the PC time series corresponding to the first EOF mode of the SLP anomalies north of the 20°N. In the low correlation models (i.e., ACCES1-0, bcc-csm1-1, CNRM-CM5, GFDL-CM3, IPSL-CM5A-LR, IPSL-CM5B-LR,
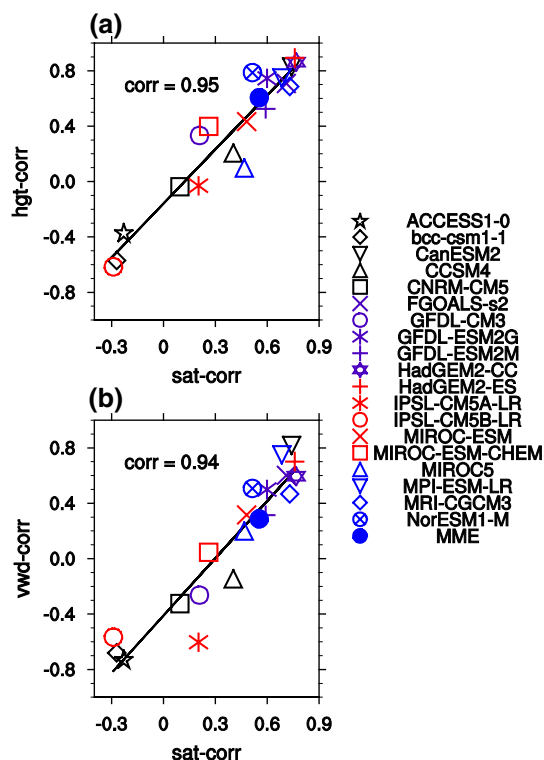
Fig. 12 Scatterplot of pattern correlation between the observed and simulated SAT anomalies vs **a** pattern correlation between the observed and simulated 500 hPa geopotential height anomalies, and **b** pattern correlation between the observed and simulated 850 hPa meridional wind anomalies over Eurasia region (40°–70°N and 0°–180°E). The best fitting line is represented by the black solid line in **a, b**
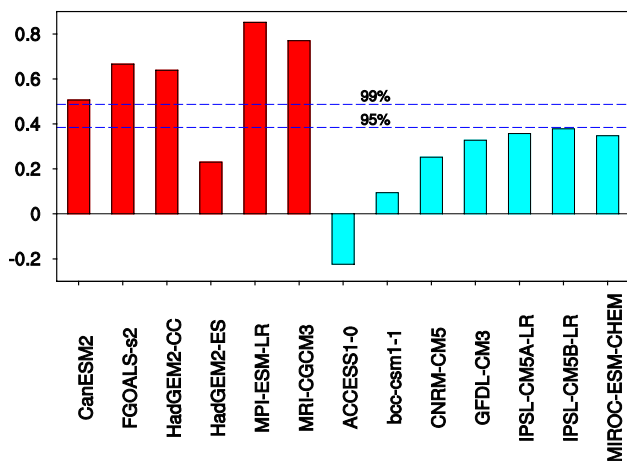

Fig. 13 Correlation coefficients between the spring AO index and the PC time series corresponding to the EOF1 of spring Eurasian SAT anomalies in the (red bars) high and (blue bars) low correlation model groups. The horizontal dashed lines indicate the correlation coefficient significant at the 95% and 99% confidence level, respectively

MIROC-ESM-CHEM), the correlations between the spring AO and the PC1 time series of the spring Eurasian SAT are all below the 95% confidence level. By contrast, in the high correlation models, except for the Had-ESM-ES, the correlations in CanESM2, FGOALS-s2, HadGEM2-CC, MPI-ESM-LR, and MRI-CGCM3 exceed the 99% confidence level. The failure of the HadGEM2-ES in reproducing the connection of between the EOF1 mode and AO may be partly due to the spatial structure of the spring AO in HadGEM2-ES that is largely different from that in the observations (not shown). Nevertheless, the above results generally indicate that a CMIP5 model's ability in reproducing the observed first EOF mode of the spring Eurasian SAT may be partly related to the model's ability in capturing its connection with the spring AO.

Besides the spring AO, Chen et al. (2016) also indicated a significant connection between the dominant modes of the spring Eurasian SAT and atmospheric circulation variations. This implies that the ability of the CMIP5 model in capturing the dominant mode of the spring Eurasian SAT may also be closely related to the model's performance in simulating the dominant mode of the spring atmospheric circulation variations over Eurasia. To address this issue, we have compared the spatial patterns corresponding to the EOF1 of the spring Eurasian 500 hPa geopotential height anomalies between the HC and LC model groups. Figure 14 displays MME anomalies of the spring 850 hPa winds and 500 hPa geopotential height anomalies obtained by regression upon the normalized PC time series of the EOF1 of spring Eurasian (40°–70°N and 0°–140°E) 500 hPa geopotential height in the HC and LC groups, respectively. There are pronounced differences in the spatial patterns of the atmospheric circulation anomalies related to the EOF1 of the spring Eurasian 500 hPa geopotential height variations. In the MME of the HC group, spatial distributions of the atmospheric circulation anomalies (i.e., 850 hPa winds and 500 hPa geopotential height) (Fig. 14a, c) bear several resemblances to those shown in Fig. 11e as well as to the observed EOF1 of spring Eurasian atmospheric anomalies (Figure S3 in the Supplementary Materials). By contrast, in the LC group, spatial patterns of the atmospheric circulation anomalies display a triple pattern, which anticyclonic and positive geopotential height anomalies over west Europe and south of the Lake Baikal and marked cyclonic and negative geopotential height anomalies over west Siberia (Fig. 14b, d). Above analysis suggests a close connection between the ability of a CMIP5 model in capturing the dominant mode of Eurasian spring SAT variations and the model's performance in reproducing the dominant mode of the spring Eurasian atmospheric variations. It should be mentioned that the spring AO may have a close connection with the dominant mode of the spring Eurasian atmospheric variability. In
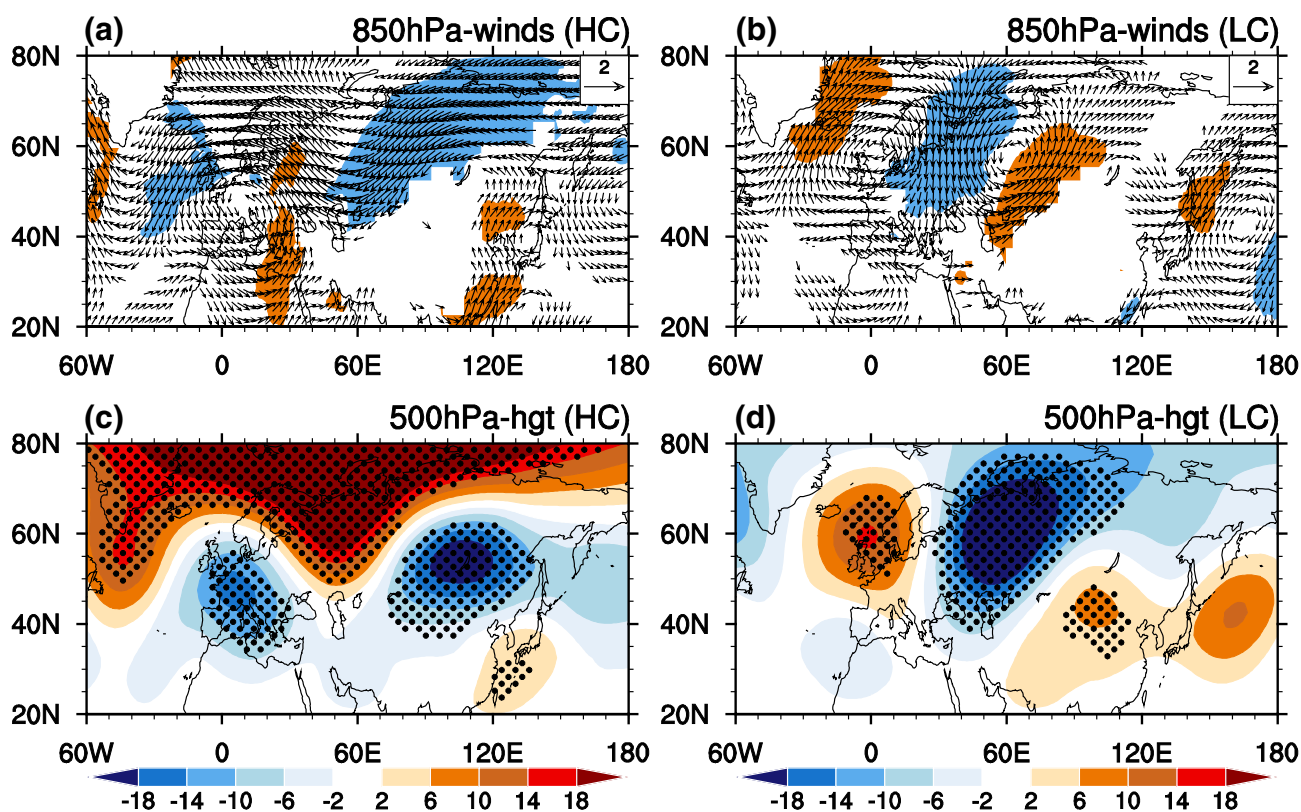
Fig. 14 MME anomalies of spring **a, b** 850 hPa winds (m s^{-1}), and **c, d** 500 hPa geopotential height (m) obtained by regression upon the normalized PC time series of the first EOF mode of spring 500 hPa geopotential height variations over Eurasia (40°–70°N and 0°–140°E) in the (left column) HC and (right column) LC groups, respectively.

Wind anomalies in **a, b** of either component that are significantly different from zero at the 95% confidence level are shaded. Geopotential height anomalies that are significantly different from zero at the 95% confidence level are stippled in **c, d**

addition, origins of the CMIP5 models' biases in capturing the spring AO and the dominant mode of the spring Eurasian atmospheric variability remain to be explored.

Previous studies showed that SST anomalies over the Pacific and North Atlantic can exert impacts on the Eurasian climate anomalies (Wu et al. 2009, 2011; Graf and Zanchettin 2012; Zhou and Wu 2016). Hence, a question is raised: whether CMIP5 models' biases in reproducing the dominant mode of the spring Eurasian SAT were related to the model's ability in capturing the relationship between the SST and the Eurasian SAT variations? Figure 15 displays MME anomalies of spring SST obtained by regression upon the normalized PC time series of the EOF1 of spring Eurasian SAT in the HC and LC groups, respectively. Spring SST anomalies are weak and insignificant in the North Atlantic, Pacific and Indian Oceans both for the HC and LC model groups (Fig. 15a, b). This indicates that the ability of the CMIP5 model in simulating the dominant mode of the spring Eurasian SAT may not due to the model's ability in capturing the relationship between the Eurasian SAT and the SST variations. This result is consistent with the observational findings obtained by Chen et al. (2016) that showed that EOF1

of spring Eurasian SAT variations has a weak correlation with SST in the Atlantic, Pacific and Indian Oceans.

5 Future projection

In this section, future changes in climatology, the standard deviation, and the leading mode of the spring SAT interannual variations over Eurasia are examined using the above selected 6 best CMIP5 models (i.e., models in the HC group). The period over 2073–2099 from RCP4.5 is analyzed to project future change. Figure 16a, b display MME climatology of spring SAT over Eurasia during the historical simulation period (1979–2005) and RCP4.5 run period (2073–2099), respectively, using the 6 best models. Figure 16c shows the differences in spring climatological SAT between historical and RCP4.5 simulations. Figure 16d, e shows standard deviations of spring SAT in the historical and RCP4.5 runs, respectively. Figure 16f displays the associated differences between the two periods.

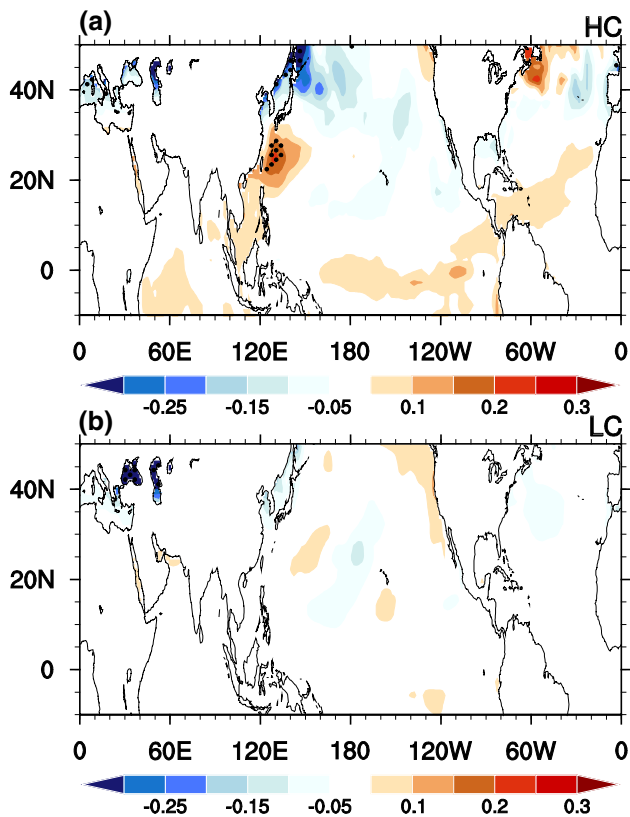The 0 °C isotherm of spring SAT in the RCP4.5 simulation is displaced northeastward compared to that in the

Fig. 15 MME anomalies of spring SST (°C) obtained by regression upon the normalized PC time series of the first EOF mode of spring Eurasian SAT variations in the **a** HC and **b** LC groups, respectively. Anomalies that are significantly different from zero at the 95% confidence level are stippled in **a, b**

historical run (Fig. 16a, b). The difference map shows that the climatological spring SAT will increase, while interannual variability of the spring SAT will decrease over most of the Eurasian continent, especially over 50°–70°N, 30°–180°E (green boxes in Fig. 16c, f). To increase robustness of the results, we have examined future changes in the climatology and standard deviation of the Eurasian spring SAT in individual CMIP5 models. Figure 17a displays differences in the climatology of spring SAT averaged over 50°–70°N, 30°–180°E (green boxes in the Fig. 16c, f) between the RCP4.5 and the historical simulations obtained in the 19 CMIP5 models. Figure 17b displays the related differences in the standard deviation of spring SAT between the RCP4.5 and the historical simulations. For the climatology of spring SAT, besides the 6 selected models (i.e., HC group, blue bars), all the other 13 models (yellow bars) also project an increase over the mid-high latitudes of the Eurasia (Fig. 17a). Furthermore, MME of the 6 selected models or MME of the 19 models also project an increase in the climatology of the Eurasian spring SAT (Fig. 17a). For the standard deviation of the spring Eurasian SAT, the 6 selected models all project a decrease (blue bars) (Fig. 17b).

In addition, 9 out of the other 13 models project a decrease (yellow bars) (Fig. 17b). Specifically, both MME of the 6 selected models and MME of the 19 models project a decrease in the standard deviation (Fig. 17b).

Xu et al. (2016) have evaluated responses of the East Asian winter monsoon to global warming in the CMIP5 models. They employed 16 models to project future change in the standard deviation of the winter SAT over East Asia and North Pacific. Their results showed that interannual variability of the winter SAT will increase over the mid-latitude of the North Pacific and the high latitude of East Asia and will decrease over the eastern China. The differences in the future change in the interannual variability of the winter and spring Eurasian SAT may be related to the differences in the background circulation change during different seasons and due to the different factors contributing to interannual variability of Eurasian SAT between the winter and spring, which remain to be explored.

In the following, we further examine the change in the leading mode of spring SAT interannual variations over the mid-high latitudes of Eurasia using the 6 best CMIP5 models. Figure 18a compares the explained variances of the first EOF mode between historical run and RCP4.5 run in the 6 best models. The explained variance of the first EOF mode will be reduced from 40.9 to 32.9% (Fig. 18a). 5 out of the 6 models project a decrease in the explained variance of the first EOF mode (Fig. 18a). Figure 18b displays the spatial pattern of the first EOF mode of Eurasian spring SAT variations during the RCP4.5 run based on the HC models. Figure 18c shows associated 500 hPa geopotential height anomalies. The spatial distribution of the spring SAT anomalies related to the first EOF mode in the RCP4.5 is similar to that in the historical run in the HC group (Figs. 11a, 18b). However, the magnitude of the negative SAT anomalies over Eurasia becomes smaller in the RCP4.5 run compared to that in the historical run. This is consistent with the weakening of the amplitude of the 500 hPa geopotential height anomalies over Eurasia (Fig. 18c). The negative geopotential height anomalies over south Europe become insignificant in the RCP4.5 run (Fig. 18c). Above results suggest that the explained variance of the first EOF mode of spring SAT over the mid-high latitudes of Eurasia will decrease in the future projection. Amplitudes of the associated atmospheric circulation and SAT anomalies will also be reduced.

6 Summary

This study analyzes the performance of 19 CMIP5 models in capturing climatology, the standard deviation, and the dominant mode of spring SAT interannual variations over the mid-high latitudes of Eurasia based on the historical
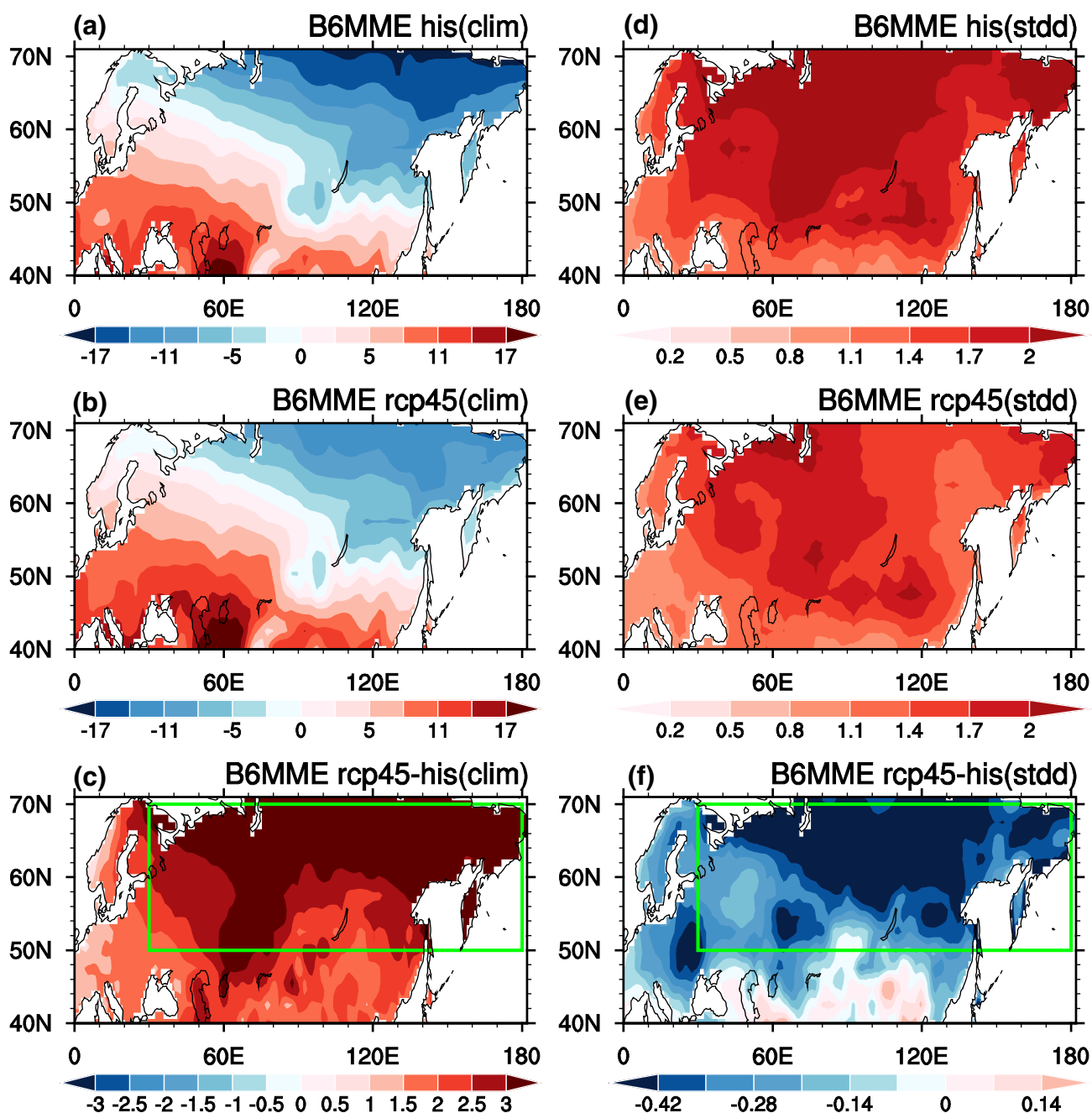
Fig. 16 MME **a** climatology (°C) and **d** standard deviation (°C) of spring SAT during 1979–2005 obtained from historical simulations of the six best models. **b** and **e** are the same as **a** and **d** but for the simulations. We also investigate future change of Eurasian spring SAT using the RCP4.5 runs.

RCP4.5 simulations during 2073–2099 based on the six best models. **c** is the difference between **b** and **a**, and **f** is the difference between **e** and **d**

The MME reproduces well the observed spatial structure of climatological spring SAT with SAT higher over southwest part of Eurasia and decreasing northeastward. The 0 °C isotherm of climatological spring SAT in MME shifts southwestward compared to that in the observations. The MME underestimates the SAT climatology over north

Europe and north Siberia by about 2.4 °C and overestimates the climatology around the Caspian Sea by about 1.8 °C. All of the 19 CMIP5 models reproduce well the spatial feature of climatological spring SAT, with the pattern correlation coefficients larger than 0.94. There exists a large spread among the 19 CMIP5 models in simulating the standard deviation of the spring SAT. Most of the models overestimate the standard deviation over the north Europe and north

Fig. 17 **a** Differences in the climatology of spring SAT (°C) averaged over 50°–70°N, 30°–180°E (i.e., green box regions in Fig. 16c, f) between the RCP4.5 simulations during period 2073–2099 and the historical simulations during period 1979–2005. Red bar indicates MME of the 6 best CMIP5 models (i.e., models in the HC group). Blue bar indicates MME of the 19 CMIP5 models. Vertical error bar indicates standard deviation of inter-model variability. **b** As in **a**, but for the differences in the standard deviation (°C) of spring SAT between the RCP4.5 simulations and the historical simulations averaged over 50°–70°N, 30°–180°E
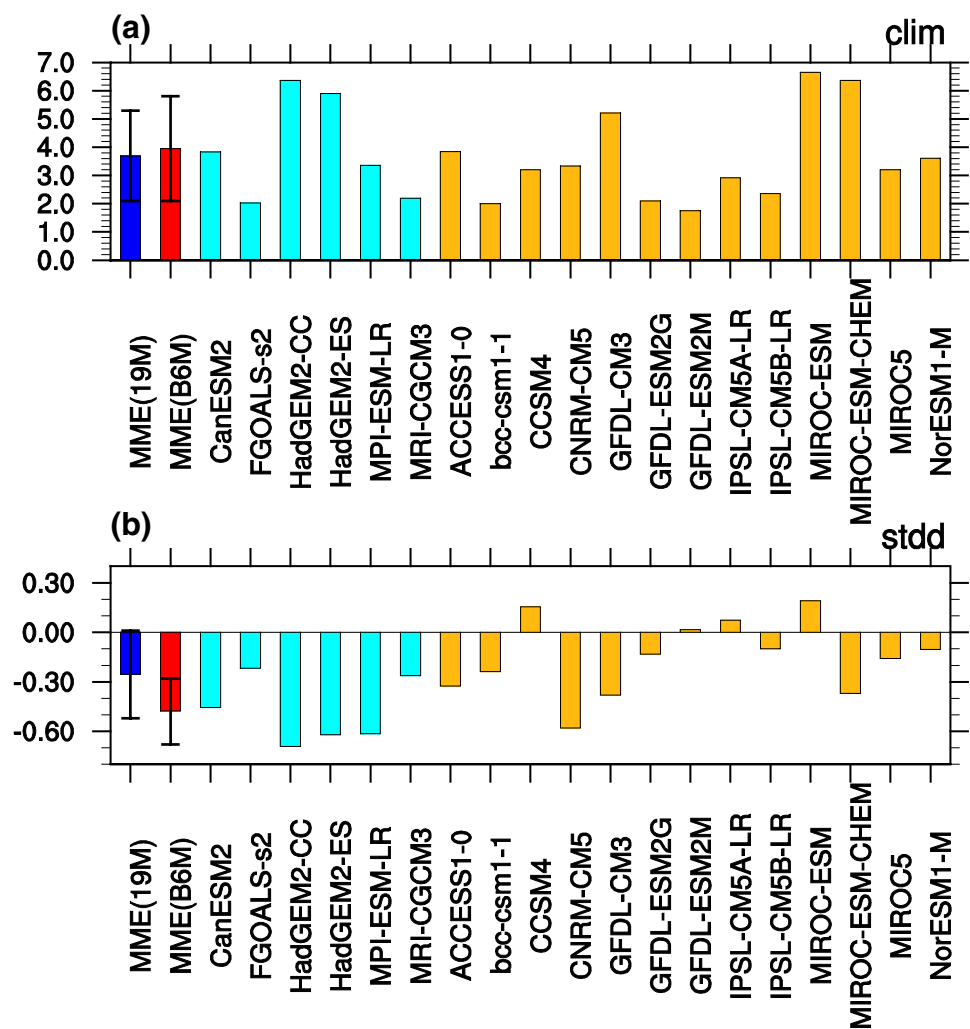
part of East Siberia, but underestimate the standard deviation over the Russian Far East. The pattern correlations of spring SAT standard deviation range from 0.22 to 0.76 in individual models, which are much larger than those of the spring climatology.

The explained variance of the dominant mode of Eurasian spring SAT variations in MME is close to that in the observations. The spatial pattern and amplitude of the spring SAT anomalies related to the first EOF mode are similar to those in the observations. There exists a large spread in reproducing the explained variance of the first EOF mode among the individual models. In particular, the explained variance of the first EOF mode is overestimated in bcc-csm1-1, GFDL-CM3, HadGEM2-CC, IPSL-CM5A-LR, MIROC-ESM-CHEM, MPI-ESM-LR, MRICGCM3, and NorESM1-M and underestimated in the other 11 CMIP5 models. Most of the models reproduce reasonably well the same-sign SAT anomalies over Eurasia related to the first EOF mode. However, the ACCESS1-0, bcc-csm1-1, GFDL-ESM2G, IPSL-CM5B-LR, and MIROC5 have a difficulty in capturing the spatial structure of the first EOF mode. Further analyses demonstrate that the ability of the CMIP5 model in reproducing the dominant mode of Eurasian spring SAT variations is closely related to the performance of the model in capturing the observed atmospheric circulation change.

Future projection of climatology, the standard deviation, and the dominant mode of the spring SAT over Eurasia is investigated using the RCP4.5 run based on six selected CMIP5 models. These six models are CanESM2, FGOALS-s2, HadGEM2-CC, HadGEM2-ES, MRI-CGCM3 and MPI-ESM-LR, which are selected based on the pattern correlation coefficients of the first EOF mode of spring SAT interannual variations. Result suggests that spring SAT will increase over most of Eurasia, especially over the north Siberia and the Russian Far East with the amplitude of warming exceeding 3 °C. However, the standard deviation of the spring SAT variations will decrease over most of Eurasia, especially over north Russia. The explained variance of the first EOF mode of spring SAT interannual variations will be reduced. In addition, amplitudes of the spring SAT and atmospheric
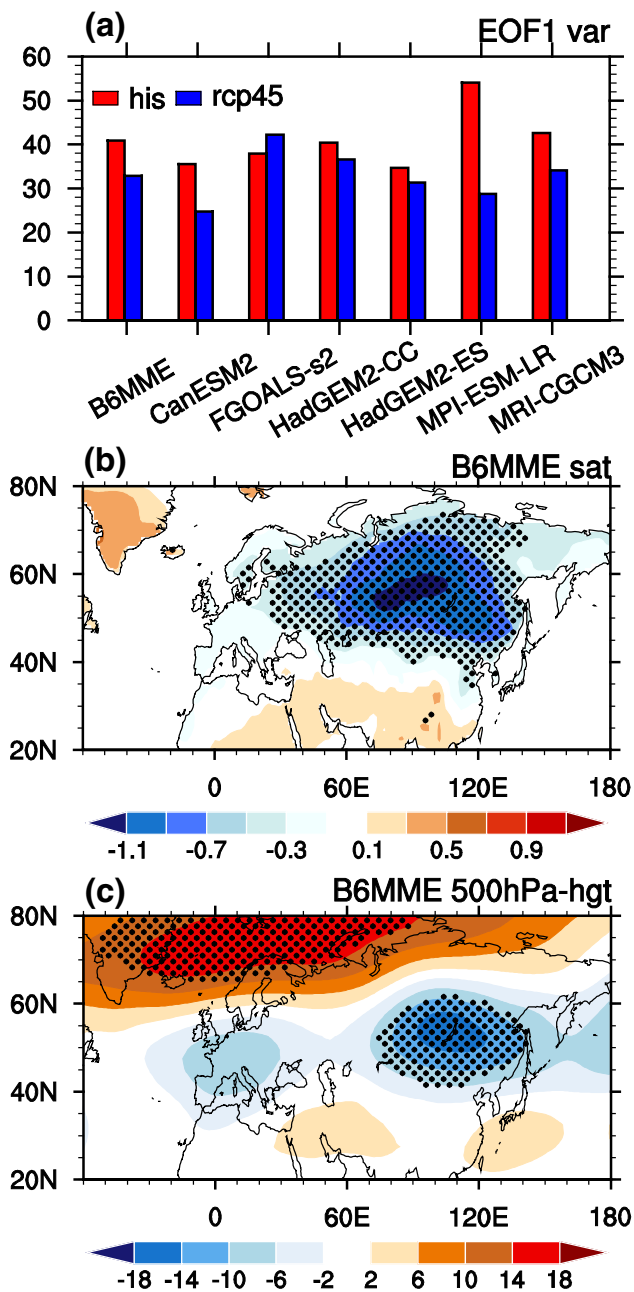
Fig. 18 a Comparison of the explained variances of the first EOF modes of spring SAT anomalies over Eurasia in historical and RCP4.5 simulations in the six best models. b MME anomalies of spring SAT (°C) obtained by regressed upon the normalized PC time series of the first EOF mode of spring SAT interannual variation over Eurasia (40°–70°N and 0°–180°E) during 2073–2099 in RCP4.5 simulations based on the six best models. c is the same as b but for MME anomalies of the 500 hPa geopotential height (m)

circulation anomalies related to the dominant mode will decrease in the future.

References

Barriopedro D, Fischer EM, Luterbacher J, Trigo RM, García-Herrera R (2011) The hot summer of 2010: redrawing the temperature record map of Europe. Science 332:220–224. https://doi.org/10.1126/science.1201224

Caloiero T (2017) Trend of monthly temperature and daily extreme temperature during 1951–2012 in New Zealand. Theor Appl Climatol 129:111–127

Chen SF, Wu R (2018) Impacts of early autumn Arctic sea ice concentration on subsequent spring Eurasian surface air temperature variations. Clim Dyn. https://doi.org/10.1007/s00382-017-4026-x

Chen SF, Yu B, Chen W (2014) An analysis on the physical process of the influence of AO on ENSO. Clim Dyn 42:973–989

Chen W, Hong X, Lu R, Jin A, Jin S, Nam J, Shin J, Goo T, Kim B (2015) Variation in summer surface air temperature over northeast Asia and its associated circulation anomalies. Adv Atmos Sci 33:1–9. https://doi.org/10.1007/s00376-015-5056-0

Chen SF, Wu R, Liu Y (2016) Dominant modes of interannual variability in Eurasian surface air temperature during boreal spring. J Clim 29:1109–1125. https://doi.org/10.1175/JCLI-D-15-0524.1

Chen SF, Chen W, Yu B (2017) The influence of boreal spring Arctic Oscillation on the subsequent winter ENSO in CMIP5 models. Clim Dyn 48:2949–2965

Cheung HN, Zhou W, Mok HY, Wu MC (2012) Relationship between Ural–Siberian blocking and the East Asian winter monsoon in relation to the Arctic Oscillation and the El Niño-Southern Oscillation. J Clim 25:4242–4257

D'Arrigo R, Wilson R, Li J (2006) Increased Eurasian-tropical temperature amplitude difference in recent centuries: Implications for the Asian monsoon. Geophys Res Lett 33:L22706. https://doi.org/10.1029/2006GL027507

Dee DP et al (2011) The ERA-Interim reanalysis: configuration and performance of the data assimilation system. Q J R Meteorol Soc 137:553–597. https://doi.org/10.1002/qj.828

Duchon C (1979) Lanczos filtering in one and two dimensions. J Appl Meteorol 18:1016–1022

Feudale L, Shukla J (2010) Influence of sea surface temperature on the European heat wave of 2003 summer. Part I: an observational study. Clim Dyn 36:1691–1703. https://doi.org/10.1007/s00382-010-0788-0

Gong DY, Wang SW, Zhu JH (2001) East Asian winter monsoon and Arctic oscillation. Geophys Res Lett 28(10):2073–2076

Graf HF, Zanchettin D (2012) Central Pacific El Niño, the "subtropical bridge", and Eurasian climate. J Geophys Res 117:D01102. https://doi.org/10.1029/2011JD016493

Guan Y, Zhang X, Zheng F, Wang B (2015) Trends and variability of daily temperature extremes during 1960–2012 in the Yangtze River Basin, China. Glob Planet Change 124:79–94

Guo Y, Zhao Z, Dong WJ (2016) Two dominant modes of winter temperature variations over China and their relationships with large-scale circulations in CMIP5 models. Theor Appl Climatol 124:579–592

Henderson-Sellers A (1996) Soil moisture: a critical focus for global change studies. Glob Planet Change 13:3–9

Huang R, Sun F (1992) Impacts of the tropical western Pacific on the East Asia summer monsoon. J Meteorol Soc Jpn 70:243–256

IPCC (2013) Summary for policymakers. Fifth Assessment Report of the Intergovernmental Panel on Climate Change. Cambridge University Press, Cambridge

Jia XJ, Lin H (2011) Influence of forced large-scale atmospheric patterns on surface air temperature in China. Mon Weather Rev 139:830–852

Kanamitsu M, Ebisuzaki W, Woollen J, Yang SK, Hnilo J, Fiorino M, Potter G (2002) NCEP–DOE AMIP-II reanalysis (R-2). Bull Am Meteorol Soc 83:1631–1643. https://doi.org/10.1175/BAMS-83-11-1631

Keellings D, Waylen P (2012) The stochastic properties of high daily maximum temperatures applying crossing theory to modeling high-temperature event variables. Theor Appl Climatol 108:579–590

Kunkel KE, Roger AP, Stanley AC (1999) Temporal fluctuations in weather and climate extremes that cause economic and human health impacts: a review. Bull Am Meteorol Soc 80:1077–1098

Li T, Du Y, Mo Y et al (2014) Human health risk assessment of heat wave based on vulnerability: a review of recent studies. J Environ Health 31:547–550 **(in Chinese)**

Liu X, Yanai M (2001) Relationship between the Indian monsoon rainfall and the tropospheric temperature over the Eurasian continent. Q J R Meteorol Soc 127:909–937. https://doi.org/10.1002/qj.49712757311

Matsueda M (2011) Predictability of Euro-Russian blocking in summer of 2010. Geophys Res Lett 38:L06801. https://doi.org/10.1029/2010GL046557

Matsuura K, Willmott CJ (2009) Terrestrial air temperature: 1900–2008 gridded monthly time series (version 4.01). University of Delaware Dept. of Geography Center. http://www.esrl.noaa.gov/psd/data/gridded/data.UDel_AirT_Precip.html. Accessed 6 Aug 2015

Miyazaki C, Yasunari T (2008) Dominant interannual and decadal variability of winter surface air temperature over Asia and the surrounding oceans. J Clim 21:1371–1386. https://doi.org/10.1175/2007JCLI1845.1

Nitta T (1987) Convective activities in the tropical western Pacific and their impact on the Northern Hemisphere summer circulation. J Meteorol Soc Jpn 65:373–390

North GR, Moeng FJ, Bell TL, Cahalan RF (1982) The latitude dependence of the variance of zonally averaged quantities. Mon Weather Rev 110:319–326

Ogi M, Tachibana Y, Yamazaki K (2003) Impact of the wintertime North Atlantic Oscillation (NAO) on the summertime atmospheric circulation. Geophys Res Lett 30:1704. https://doi.org/10.1029/2003GL017280

Stott PA, Stone DA, Allen MR (2004) Human contribution to the European heatwave of 2003. Nature 432:610–614. https://doi.org/10.1038/nature03089

Sun J, Wang H, Yuan W (2008) Decadal variations of the relationship between the summer North Atlantic Oscillation and middle East Asian air temperature. J Geophys Res 113:D15107

Sun Y, Zhang X, Zwiers F, Song L, Wan H, Hu T, Yin H, Ren G (2014) Rapid increase in the risk of extreme summer heat in Eastern China. Nat Clim Change 4:1082–1085

Taylor KE (2001) Summarizing multiple aspects of model performance in a single diagram. J Geophys Res 106:7183–7192

Taylor KE, Stouffer RJ, Meehl GA (2012) An overview of CMIP5 and the experiment design. Bull Am Meteorol Soc 93(4):485–498

Thompson DW, Wallace JM (1998) The Arctic Oscillation signature in the wintertime geopotential height and temperature fields. Geophys Res Lett 25:1297–1300. https://doi.org/10.1029/98GL00950

Thomson AM, Calvin KV, Smith SJ, Kyle GP, Volke A, Patel P, Delgado-Arias S, Bond-Lamberty B, Wise MA, Clarke LE (2011) RCP4.5: a pathway for stabilization of radiative forcing by 2100. Clim Change 109(1):77–94

Wang B, Wu ZW, Chang CP, Liu J, Li J, Zhou T (2010) Another look at interannual-to-interdecadal variations of the East Asian winter monsoon: the northern and southern temperature modes. J Clim 23:1495–1512

Webster PJ, Yang S (1992) Monsoon and Enso: selectively interactive systems. Q J R Meteorol Soc 118(507):877–926

Wu R, Chen SF (2016) Regional change in snow water equivalent–surface air temperature relationship over Eurasia during boreal spring. Clim Dyn 47:2425–2442

Wu B, Wang J (2002) Winter Arctic oscillation, Siberian high and East Asian winter monsoon. Geophys Res Lett 29(19):1897. https://doi.org/10.1029/2002GL015373

Wu ZW, Wang B, Li J, Jin FF (2009) An empirical seasonal prediction model of the East Asian summer monsoon using ENSO and NAO. J Geophys Res 114:D18120. https://doi.org/10.1029/2009JD011733

Wu R, Yang S, Liu S, Sun L, Lian Y, Gao Z (2011) Northeast China summer temperature and North Atlantic SST. J Geophys Res 116:D16116. https://doi.org/10.1029/2011JD015779

Wu ZW, Zhang P, Chen H, Li Y (2016) Can the Tibetan Plateau snow cover influence the interannual variations of Eurasian heat wave frequency? Clim Dyn 46:3405–3417

Xia JJ, Tu K, Yan ZW, Qi Y (2016) The super-heat wave in eastern China during July–August 2013: a perspective of climate change. Int J Climatol 36:1291–1298

Xu MM, Xu HM, Ma J (2016) Responses of the East Asian winter monsoon to global warming in CMIP5 models. Int J Climatol 36:2139–2155

Yao PZ (1995) The climate features of summer low temperature cold damage in northeast China during recent 40 years. J Catastrophol 10:51–56 **(in Chinese)**

Ye L, Yang G, Van Ranst E, Tang H (2013) Time-series modeling and prediction of global monthly absolute temperature for environmental decision making. Adv Atmos Sci 30:382–396

Zeng J, Zhai Y, Wu Z, Hu K (2011) Effects of high temperature in summer on yield and its components in bitter gourd with 15 cross combinations and strains. Chin J Trop Crops 32:2025–2028 **(in Chinese)**

Zhou Y, Wu ZW (2016) Possible impacts of mega-El Niño/Southern Oscillation and Atlantic multidecadal oscillation on Eurasian heat wave frequency variability. Q J R Meteorol Soc 142:1647–1661

Zuo J, Ren HL, Wu BY, Li WJ (2016) Predictability of winter temperature in China from previous autumn Arctic sea ice. Clim Dyn 47:2331–2343

Zveryaev II, Gulev SK (2009) Seasonality in secular changes and interannual variability of European air temperature during the twentieth century. J Geophys Res 114:D02110. https://doi.org/10.1029/2008JD010624